DESIGN CONCEPT OF CERAMIC CHAMBERS AT THE J-PARC RCS: AN ANALYTICAL PERSPECTIVE

Y. Shobuda*, Japan Proton Accelerator Research Complex, Tōkai Mura, Japan
M. Kinsho, Japan Atomic Energy Agency, Tōkai Mura, Japan
T. Toyama, High Energy Accelerator Research Organization, Tsukuba, Japan

Abstract

Ceramic chambers are essential for rapidly accelerating high-intensity beams, as they mitigate eddy current effects. Although computer simulations and precise measurements are required to validate the estimates, analytical perspectives provide valuable insights into chamber design. Specifically, the configuration of bending magnets and chambers is vital to minimizing beam loss at the injection area.

INTRODUCTION

The 3-GeV RCS (Rapid Cycling Synchrotron) [1] at J-PARC [2] is a proton accelerator to achieve a 1-MW beam by accelerating two bunches containing $N_b = 4.15 \times 10^{13}$ particles per bunch (ppb) from 400 MeV to 3 GeV in 20 ms with a repetition rate of 25 Hz without any transverse feedback [3, 4].

The developed ceramic chambers [5], shown in Fig. 1 [6], are installed in all magnets of the RCS. The outer surface of the ceramic chamber, with radius a_{II}, is covered with N rectangular copper strips (RF shields) with a horizontal width h_x and radial thickness t. Each strip is terminated at one end by capacitors. The inner surface, with radius a_I, is coated with a titanium nitride (TiN) layer of thickness Δ. These TiN-coated ceramic chambers are essential for rapidly accelerating high-intensity beams within 20 ms, as they mitigate eddy current effects in the chamber and suppress secondary electron emissions caused by the proton beam halo colliding with the chamber surface, thereby avoiding electron cloud instability [7].

An analytical study could provide valuable insights for designing ceramic chambers to assist in developing the next generation, backed by the success of the J-PARC RCS [3].

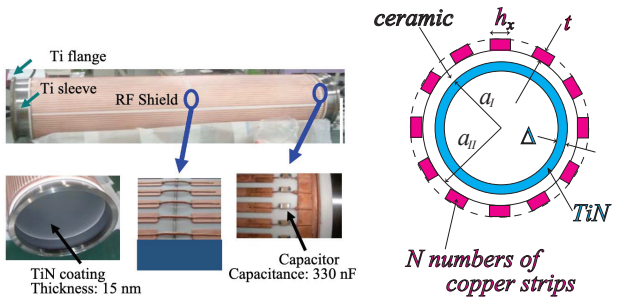

Figure 1: A ceramic chamber covered with RF shields (copper strips).

* yoshihiro.shobuda@j-parc.jp

DESIGN CONCEPT IN TERMS OF BEAM IMPEDANCE AND CHAMBER HEATING

Determination of the Thickness of RF Shields

Since the electromagnetic screening effect is a crucial factor in designing RF shields, the thickness t of the shields is determined by taking into account the leakage field from the chamber [8].

For simplicity, let us consider a cylindrical metal chamber of length g with conductivity σ_c, where the inner radius and thickness are a_{II} and t, respectively. From this standpoint, it is essential to consider the acceleration of 'non-relativistic' beams with Lorentz-β and -γ at the RCS. Consequently, the general form of the resistive-wall impedance, excluding the space charge impedance [9, 10], is simplified as [11],

$$Z_L \simeq \frac{\nu_2 g}{2a_{II}\pi\sigma_c \tanh(\nu_2 t)}, \tag{1}$$

for non-relativistic beams in the frequency range of

$$\frac{\frac{c\beta^2\gamma^2}{2\pi t\sigma_c Z_0 (a_{II}+t)\left|\Gamma+\log[\frac{(a_{II}+t)}{t^2\beta\gamma Z_0\sigma_c}]\right|}}{\sqrt{[1+\frac{t\beta^2\gamma^2}{(a_{II}+t)(\Gamma+\log[\frac{(a_{II}+t)}{t^2\beta\gamma Z_0\sigma_c}])}]}} \lesssim f < \frac{c}{\pi t^2 Z_0 \sigma_c}, \tag{2}$$

where c is the velocity of light, $k = \omega/c\beta$, $Z_0 = 120\pi$ [Ω], $\nu_2 = \sqrt{k^2 + jk\beta Z_0\sigma_c}$, and Euler's constant: $\Gamma = 0.577216$. Note that Eq. (1) reduces to the DC resistance when the skin depth is larger than t, implying that the wall currents shield the electromagnetic field of the non-relativistic beam.

Figure 2 illustrates the outcomes for the parameters t = 0.5 mm, $\sigma_c = 5.9 \times 10^7$ S/m, a_{II} = 157.7 mm, g = 0.86 m, and Lorentz-β = 0.97. The red, blue, green, and black lines represent the exact result of the resistive-wall impedance [9, 10], the exact result for an infinite t, Eq. (1), and the DC resistance, respectively. Equation (1) reproduces the exact result well. When the skin depth exceeds t ($f \lesssim 17$ kHz), the impedance approaches the DC resistance until the frequency becomes extremely low, around 50 Hz. Finally, whether this low-frequency limit is sufficient to shield the electromagnetic fields was validated by measurements [12].

Determination of Strip Area Ratio

The area ratio $\theta = Nh_x/2\pi a_{II}$ covered by N strips is determined from the space-charge impedance [13] of a chamber composed of the strips, neglecting the contribution of the TiN-coated ceramic [8].

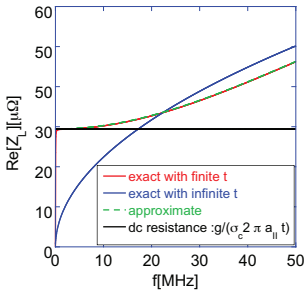

Figure 2: Impedance of a cylindrical chamber.

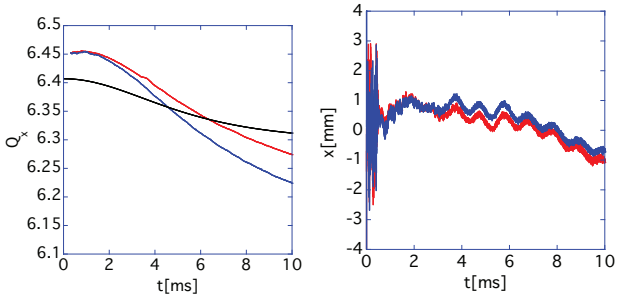

Figure 3: Tune-tracking patterns and beam positions [4].

Reference [14] provides the space-charge impedance of N strips covered by a cylindrical ceramic pipe with inner radius r_i and a conducting pipe with inner radius r_t. By taking the radii r_i and r_t to infinity, we can extract the impedance of a chamber composed solely of the strips, expressed as:

$$Z_L = \frac{j\omega R Z_0}{2c\beta^2\gamma^2}\left[2\log[\frac{a_{II}}{r_b}] + (1 - \frac{2}{N}\log[\theta])\right], \quad (3)$$

where r_b is the radial beam size, and R is the average radius of the RCS circumference.

When the condition

$$\frac{2}{N}\log(\theta) \ll 1, \quad (4)$$

is satisfied, Eq. (3) reproduces the space-charge impedance of a cylindrical chamber with inner radius a_{II} [13]. Therefore, we can set $\theta = 0.5$ and $N \simeq 100$ as parameters after the horizontal width h_x is determined by the heating condition due to eddy currents in the strips [8].

Determination of the Capacitance

The capacitance is typically determined by the condition that the impedance must be low for the circulating beam and high for the induced current at the frequency components of the time-dependent external magnetic field [15]. Since the RCS accelerates the beam at a repetition rate of 25 Hz, a capacitance of 330 nF was chosen.

However, the RF-shielded ceramic chamber functions as an LCR circuit together with both end flanges [15]. Analytical calculations reveal the intrinsic frequencies of the RF-shielded chamber, showing a maximum frequency of approximately 250 kHz [15]. Therefore, we must consider the field modulations ΔB when the sinusoidal external magnetic field B_{ext} is applied during acceleration. These modulations are evaluated as $\Delta B/B_{ext} < 2 \times 10^{-7}$ [15], which is negligible for the RCS.

For validation, beam position measurements were performed with different tune-tracking patterns during acceleration [4], as shown by the red and blue lines up to 10 ms in the left panel of Fig. 3. The resonance line originating from 250 kHz is overlaid in black. The right panel shows the horizontal beam positions for a 1-MW beam (4.15×10^{13} ppb) under the respective tune-tracking patterns, using the same color scheme as the left panel. Although the red and blue tune-tracking lines cross the resonance line at approximately 6 ms and 4.5 ms, respectively, no beam instability or beam loss is observed in the right panel [4]. Measurements confirm negligible field modulation during acceleration.

Determination of the Horizontal Width

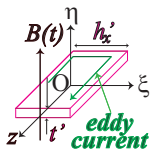

Figure 4: Strip perpendicular to the dipole magnetic field.

Thanks to the capacitors, the heating contribution from the RLC circuit comprising the strips and flanges to the ceramic chamber is negligible.

The dominant contribution to heating comes from the inner part of the strip. Here, let us consider a strip with vertical size t' and horizontal size h'_x, oriented perpendicular to the dipole magnetic field, as shown in Fig. 4. The eddy current density i_z at (ξ, η, z) within the strip is given by [15]:

$$i_z(\xi,\eta,z) = \frac{16c}{Z_0 h_x'^2}\int_{-\infty}^{t} dt' \frac{dB(t')}{dt'} e^{\frac{16c}{Z_0 h_x'^2 \sigma_c}(t'-t)}\xi. \quad (5)$$

For a 1-m-long strip with $h'_x = 5$ mm and $t' = 0.5$ mm that experiences maximum eddy-current heating among all strips, the power consumption due to the eddy currents is estimated to be approximately 0.5 W under 25-Hz operation.

Determination of the Thickness of TiN coating

To prevent electron cloud instabilities [7], the secondary electron emission yield coefficient δ of the material on the chamber's inner surface must be below 1. It was expected that δ could be reduced below 1 when the TiN coating thickness Δ exceeds 0.5 nm [8]. In addition, a significant reduction was observed for a TiN coating of 1-2 nm [5, 16]. Furthermore, TiN suppresses the diffusion of adsorbed gases from the inner ceramic walls to the surface, as well as moisture adsorption on the chamber surface [17].

On the other hand, the constraint from the impedance budget must be considered to avoid beam instabilities [6, 18]. By generalizing the model presented in [14], we can evaluate the impedance of the ceramic chamber with a TiN

coating. Consequently, the ceramic chamber for the RCS can be approximated as a multi-layered chamber composed of TiN, ceramic, and conductive pipes in the radial direction [19], producing the impedance [20, 21]:

$$Z_L \simeq \frac{gZ_0}{2\pi\beta a_I\left[Z_0\Delta\sigma_{TiN} - \frac{j\epsilon'}{(\epsilon'\beta^2-1)ka_I\log[\frac{a_{II}}{a_I}]}\right]}, \quad (6)$$

where σ_{TiN} is the conductivity of TiN, and ϵ' is the relative dielectric constant of the ceramic. A thinner TiN coating is preferable from an impedance perspective because the wall currents flow predominantly on the RF shields as Δ approaches zero. In the end, the thickness of the TiN coating is determined to be 15 nm by the impedance budget [6].

Comparison to the Measurements

To validate the analytical estimate, we compare Eq. (6) with measurements obtained via the standard wire method [22], as reported in Ref. [6], where Lorentz-β = 1, a_I = 149.5 mm, a_{II} = 157.7 mm, g = 0.86 m, Δ = 15 nm, $\sigma_{TiN} = 5.88 \times 10^6$ S/m, and $\epsilon' = 11$.

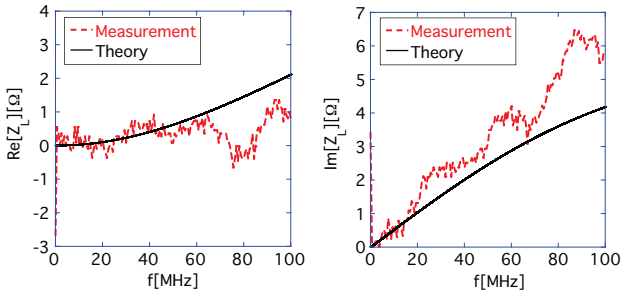

Figure 5: Longitudinal impedance (theory/measurement).

As shown in Fig. 5, the theoretical results from Eq. (6) (solid) agree well with measurements (dashed) up to at least 100 MHz, which suffices for the RCS longitudinal beam size. Furthermore, the beam-induced heating is estimated at ~0.5 W per chamber based on the longitudinal impedance. This estimate, even combined with eddy-current heating, remains well within the acceptable limit for the RCS.

MITIGATION OF RESONANCE LOSSES AND HEATING RATE ASSOCIATED WITH THE INJECTION SCHEME

A special design is required for the RCS injection section [23, 24], where the H^- injection and circulating proton beams merge under a trapezoidal magnetic field (Fig. 6), because the field modulation from each chamber's LCR circuit is estimated at $dB/B_{ext} > 0.018$ [15].

To accumulate beams during injection, four bump magnets (two opposite-polarity pairs) are excited. If all magnets, including chambers, are identical and share a single power supply, the dipole kicks from field errors perfectly cancel out, leaving the circulating beams unaffected and eliminating resonance effects [25].

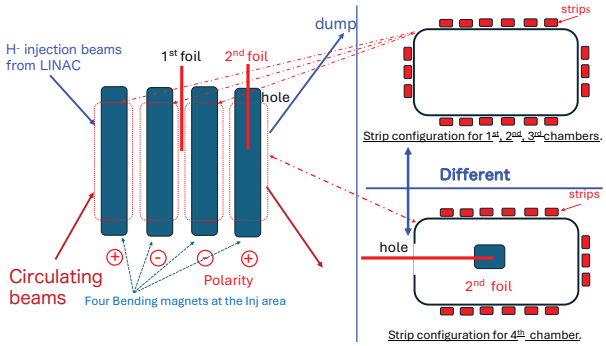

Figure 6: Injection section of the RCS [23, 24] and the chambers located there.

The critical importance of this identical configuration, including chambers, was confirmed experimentally when several capacitors on the rectangular chambers failed due to insufficient voltage durability and became partially detached while the injection beam energy was 181 MeV [26]. Following this detachment, significant beam losses were observed at $\nu_x = \nu_y = 6.2$ during the injection period—including during the ramp-down of the trapezoidal waveform—even for a lower-intensity beam of 4.2×10^{11} ppb [26].

Analytical calculations revealed that after passing through all four bending magnets, the 181-MeV beams effectively experienced a field error at a frequency of 100 kHz. This error was attributed to asymmetry among the RF-shielded chambers, causing the beam losses at $\nu_x = \nu_y = 6.2$ [25].

Even after the identical configuration among the four chambers was partially restored following the 400-MeV injection energy upgrade [1], beam loss is still observed at $\nu_x = 6.14$. This is close to the theoretical prediction of $\nu_x = 6.13$ [25], which arises because the RF shields are completely removed from one of the four outer surfaces of the fourth chamber to allow the insertion of the second foil (Fig. 6). However, this resonance tune is irrelevant to high-intensity beam operations because the operational tune is chosen far from the integer tune $\nu_x = 6.0$ [4].

Regarding the thermal aspects, the heating rate due to eddy currents is estimated to be only 0.5 W per chamber following the procedure described above. This is attributed to the strip dimension, which is $h'_x = 5$ mm and $t' = 0.5$ mm on the top and bottom surfaces, and $h'_x = 0.5$ mm and $t' = 5$ mm on the left and right surfaces of the chamber, consistent with simulations [15].

SUMMARY

The analytical design of the ceramic chamber can be performed by considering the shielding effects on radiation fields, the sufficient suppression of beam impedance, the buildup of electron cloud, and the heating rate due to beams and eddy currents excited by external fields. This serves as an effective guideline for preliminary parameter determination, although numerical simulations and experimental measurements are required for precise validation.

REFERENCES

[1] K. Yamamoto *et al.*, "Design and actual performance of J-PARC 3 GeV rapid cycling synchrotron for high-intensity operation", *J. Nucl. Sci. Technol.*, vol. 59, p. 1174, 2022. doi:10.1080/00223131.2022.2038301

[2] J-PARC, "Japan Proton Accelerator Research Complex", http://j-parc.jp/index-e.html,

[3] J-PARC Center, "J-PARC Annual Report 2014", http://j-parc.jp/documents/annual_report/a_report_2014.pdf, p. 9, 2015,

[4] Y. Shobuda *et al.*, "Theoretical elucidation of space charge effects on the coupled-bunch instability at the 3 GeV rapid cycling synchrotron at the Japan Proton Accelerator Research Complex", *Prog. Theor. Exp. Phys.*, vol. 2017, no. 1, 013G01, 2017. doi:10.1093/ptep/ptw169

[5] M. Kinsho *et al.*, "Development of alumina ceramics vacuum duct for the 3 GeV-RCS of the J-PARC project", *Vacuum*, vol. 73, p. 187, 2004. doi:10.1016/j.vacuum.2003.12.043

[6] Y. H. Chin, S. Lee, Y. Shobuda, K. Takata, T. Toyama, and H. Tsutsui, "Impedance and radiation generated by a ceramic chamber with RF shields and TiN coating", in *Proc. HB2006*, paper TUBX01, pp. 125–127, 2006.

[7] K. Ohmi, T. Toyama, and C. Ohmori, "Electron cloud instability in high intensity proton rings", *Phys. Rev. Spec. Top. Accel. Beams*, vol. 5, p. 114402, 2002. doi:10.1103/PhysRevSTAB.5.114402

[8] Y. Saito, "Memorandum", Unpublished, in Japanese, 2003,

[9] E. Metral, B. Salvant, and B. Zotter, "Resistive-Wall Impedance of an Infinitely Long Multi-Layer Cylindrical Beam Pipe", in *Proc. PAC'07*, pp. 4216–4218, 2007. doi:10.1109/pac.2007.4439984

[10] Y. Shobuda, "OHO'10", Eq. (2.15), Tsukuba, Aug. 2010, 2010, http://accwww2.kek.jp/oho/OHO%20text%20archives%202005-2011/OHO10%20web%20final/OHO10_shobuda_20100816.pdf,

[11] Y. Shobuda, "Two-dimensional resistive-wall impedance with finite thickness: Its mathematical structures and their physical meanings", *Prog. Theor. Exp. Phys.*, vol. 2022, no. 5, 053G01, 2022. doi:10.1093/ptep/ptac053

[12] S. Hiramatsu, "Response to the loop antenna", Unpublished, in Japanese, 2005,

[13] A. W. Chao, *Physics of Collective Beam Instabilities in High Energy Accelerators*. New York: Wiley, 1999.

[14] T.-S. F. Wang, S. S. Kurennoy, and R. L. Gluckstern, "Space-charge impedance of rf-shielding wires with external ceramic and conducting pipes", *Phys. Rev. Spec. Top. Accel. Beams*, vol. 4, p. 104201, 2001. doi:10.1103/PhysRevSTAB.4.104201

[15] Y. Shobuda, Y. Irie, and S. Igarashi, "Analytical method for the evaluation of field modulation inside the rf-shielded chamber with a time-dependent dipole magnetic field", *Phys. Rev. Spec. Top. Accel. Beams*, vol. 12, p. 032401, 2009. doi:10.1103/PhysRevSTAB.12.032401

[16] S. Michizono, A. Kinbara, Y. Saito, S. Yamaguchi, S. Anami, and N. Matuda, "TiN film coatings on alumina radio frequency windows", *J. Vac. Sci. Technol. A*, vol. 10, p. 1180, 1992. doi:10.1116/1.578223

[17] H. Kato *et al.*, "TiN Coating on Inside of Pipe by Hollow Cathode Discharge Process", *Vacuum*, vol. 38, p. 380, 1995. doi:10.3131/jvsj.38.380

[18] Y. H. Chin, J. Kamiya, Y. Shobuda, K. Takata, and T. Toyama, "Impedance and Beam Instability Issues at J-PARC Rings", in *Proc. HB2008*, paper WGA01, pp. 40–44, 2008. https://accelconf.web.cern.ch/HB2008/papers/wga01.pdf

[19] Y. Shobuda, Y. H. Chin, K. Ohmi, and T. Toyama, "The Impedance of the Ceramic Chamber in J-PARC", in *Proc. PAC'05*, pp. 1898–1900, 2005. doi:10.1109/PAC.2005.1590950

[20] S. Lee, "Simplified Z_L model of the ceramic pipe in RCS", Internal Report, in Japanese, 2003,

[21] Y. Shobuda, Y. H. Chin, and K. Takata, "Impedance of a ceramic break and its resonance structures", *Phys. Rev. Spec. Top. Accel. Beams*, vol. 17, p. 091001, 2014. doi:10.1103/PhysRevSTAB.17.091001

[22] *Handbook of Accelerator Physics and Engineering*, A. W. Chao and M. Tigner, Eds. Singapore: World Scientific, 1999.

[23] I. Sakai *et al.*, "H- Painting Injection System for the JKJ 3 GeV High Intensity Proton Synchrotron", in *Proc. EPAC'02*, paper THPLE007, pp. 1040–1042, 2002.

[24] P. K. Saha *et al.*, "Direct observation of the phase space footprint of a painting injection in the Rapid Cycling Synchrotron at the Japan Proton Accelerator Research Complex", *Phys. Rev. Spec. Top. Accel. Beams*, vol. 12, p. 040403, 2009. doi:10.1103/PhysRevSTAB.12.040403

[25] Y. Shobuda and Y. Irie, "Analytical Estimation of the Field Modulation during the Injection Period of the 3 GeV RCS in J-PARC", *JPS Conf. Proc.*, vol. 8, p. 012003, 2015. doi:10.7566/JPSCP.8.012003

[26] H. Hotchi *et al.*, "Beam commissioning of the 3-GeV rapid cycling synchrotron of the Japan Proton Accelerator Research Complex", *Phys. Rev. Spec. Top. Accel. Beams*, vol. 12, p. 040402, 2009. doi:10.1103/PhysRevSTAB.12.040402